

# Water Resources Research®



## RESEARCH ARTICLE

10.1029/2024WR037826

# A New Model for Water Retention and Hydraulic Conductivity Curves of Deformable Unsaturated Soils

Zhenxing Chang<sup>1</sup>  and Chao Zhou<sup>1</sup> 

<sup>1</sup>Department of Civil and Environmental Engineering, The Hong Kong Polytechnic University, Hung Hom, Hong Kong

### Key Points:

- A new equation was proposed to model the evolution of pore size distribution with soil density
- The water retention model captures the increase of not only air-entry value but also adsorption/desorption rate with increasing density
- The hydraulic conductivity model considers the evolution of pore size distribution and tortuosity upon soil deformation

### Correspondence to:

C. Zhou,  
c.zhou@polyu.edu.hk

### Citation:

Chang, Z., & Zhou, C. (2025). A new model for water retention and hydraulic conductivity curves of deformable unsaturated soils. *Water Resources Research*, 61, e2024WR037826. <https://doi.org/10.1029/2024WR037826>

Received 30 APR 2024

Accepted 14 APR 2025

### Author Contributions:

**Conceptualization:** Chao Zhou  
**Data curation:** Zhenxing Chang  
**Funding acquisition:** Chao Zhou  
**Methodology:** Zhenxing Chang  
**Supervision:** Chao Zhou  
**Validation:** Zhenxing Chang  
**Visualization:** Zhenxing Chang  
**Writing – original draft:** Zhenxing Chang  
**Writing – review & editing:** Zhenxing Chang, Chao Zhou

**Abstract** The water retention and hydraulic conductivity curves of unsaturated soils are important parameters for seepage analysis. Experimental results in the literature generally show that with increasing density, the air-entry value and adsorption/desorption rate of the water retention curve increase and the relative hydraulic conductivity ( $k_r$ ) at a given degree of saturation changes. The above phenomena, except the density-dependency of air-entry value, have not been considered in existing models. This study aims to address these problems by developing new hydraulic models based on experimental evidence from microscopic analysis. First of all, a new equation was proposed to model the evolution of pore size distribution with soil density. For a given pore, the ratio of its initial to final sizes is higher when the initial size is larger and when there is a greater increase in density. Based on this equation, a new and simple water retention equation was derived to predict the increase in air-entry value (resulting from the reduction in pore size) and the adsorption/desorption rate (due to a more uniform pore size distribution) as density increases. Then, a new equation for  $k_r$  was developed by incorporating the evolution of pore size distribution and tortuosity upon soil deformation, and therefore it can capture the changes of  $k_r$ . To validate the above equations, test data from several soils with distinct properties were used. The measured and calculated results are well-matched.

## 1. Introduction

The hydraulic properties of unsaturated soils play a pivotal role in the transient seepage analysis and the management of underground water resources (Fan et al., 2019; Fu et al., 2023), including the water retention curve (the relationship between the water content or degree of saturation and pressure head) and the relative hydraulic conductivity curve (the relationship between relative hydraulic conductivity and the water content, degree of saturation or pressure head) (Fredlund & Rahardjo, 1993; Ng et al., 2024). The relative hydraulic conductivity  $k_r$  is defined as the ratio of unsaturated soil's hydraulic conductivity to the saturated soil's hydraulic conductivity, falling from 0 to 1. The water retention and relative hydraulic conductivity curves are governed by the microstructure of soils (e.g., pore size distribution and tortuosity) that varies with soil deformation under various mechanical and hydraulic loadings, such as traffic loads, compaction, and wetting-drying cycles. Consequently, investigating the impact of soil density on the hydraulic properties of unsaturated soils is important.

So far, extensive experimental studies of water retention and relative hydraulic conductivity curves have been reported in the literature. On the one hand, the water retention curve is often characterized by its air-entry value, adsorption/desorption rate, size of the hysteresis loop, and residual water content (Fredlund et al., 2011). Test data consistently led to the conclusion that an increase in soil density (i.e., void ratio reduction) results in a higher air-entry value and an increased water retention capacity (Bella, 2021; Lee et al., 2005; Moghaddasi et al., 2017; Ng & Pang, 2000; Ng & Peprah-Manu, 2023; Sun & Sun, 2012). Moreover, when soil becomes denser, there is an increase in the adsorption and desorption rates (i.e., the slope of the measured water retention curve in the  $S_r$ - $\ln(h)$  plane, where  $S_r$  is the degree of saturation,  $h$  is the pressure head) for many soils (e.g., Bella, 2021; Romero, 1999; Romero et al., 1999), as shown in Figure 1a, even though the change is not very obvious for some other soils. On the other hand, the measured  $k_r$  at a given degree of saturation changes with an increase in density (Nemes et al., 2015), as shown in Figure 1b, or remains almost constant (Laliberte et al., 1966).

From the perspective of modeling, many models for the water retention curve have been reported in the literature (Assouline et al., 1998; Fredlund & Xing, 1994; Gallipoli et al., 2003; Kosugi, 1994; Li et al., 2023; van Genuchten, 1980; Wang et al., 2025; Zhou & Chen, 2021; Zhou & Ng, 2014). For example, the widely used VG model (van Genuchten, 1980) can be expressed as

© 2025. The Author(s).

This is an open access article under the terms of the [Creative Commons Attribution License](https://creativecommons.org/licenses/by/4.0/), which permits use, distribution and reproduction in any medium, provided the original work is properly cited.

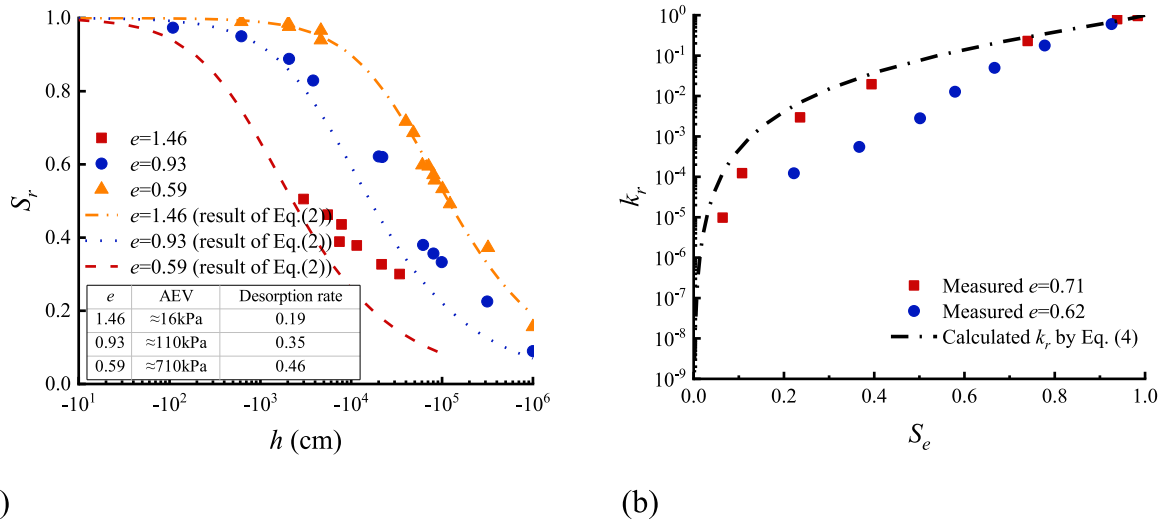


**Figure 1.** Experimental observation of density effects on hydraulic properties and predictions by existing models: (a) water retention curve (test data from Romero (1999)); (b) relative hydraulic conductivity curve (test data from Nemes et al. (2015)).

$$S_r = [1 + (\alpha h)^n]^{-m} \quad (1)$$

where  $\alpha$  is a parameter related to air-entry value,  $n$  and  $m$  are parameters related to pore size distribution. The predicted relationship between  $S_r$  and  $h$  using Equation 1 is density-independent and inconsistent with the findings in Figure 1a. To address this problem, Gallipoli et al. (2003) proposed a semi-empirical power function to model the relationship between void ratio ( $e$ ) and  $\alpha$  based on the experimental results:  $\alpha = \phi e^\psi$ , where  $\phi$  and  $\psi$  are model parameters. Then, Equation 1 can be derived as follows:

$$S_r = [1 + (\phi e^\psi h)^n]^{-m} \quad (2)$$

A similar water retention model was established by Tarantino (2009) by analyzing the experimental results of two reconstituted soils and two compacted soils. To better understand the density effect on the water retention curve, Hu et al. (2013) considered the evolution of pore size distribution under deformation since pore size distribution strongly correlates with the water retention curve. Pore size distribution can be determined by mercury intrusion porosimetry (MIP) tests (Li & Zhang, 2009; Tanaka et al., 2003; Wang et al., 2020). Hu et al. (2013) proposed a simple method to describe the evolution of pore size distribution with void ratio. It was assumed that upon soil deformation, all the pore sizes are reduced by the same ratio (i.e., the initial and final pore sizes are independent of the initial pore size). This ratio is a function of the reduction in void ratio. Based on this simplified method of modeling pore size distribution evolution, Equation 3 was derived to describe a density-dependent water retention curve:

$$S_r = [1 + \{\beta \exp[-k_p(e - e_0)]h\}^n]^{-m} \quad (3)$$

where  $e$  and  $e_0$  are current and initial void ratios,  $\beta$  is a parameter related to air-entry value, and  $k_p$  is a parameter governing the influence of void ratio on pore size and the air-entry value. Even though Equations 2 and 3 were derived from different approaches, their modeling capabilities are comparable. Both predict shifting the water retention curve in the  $S_r$ - $\ln(h)$  plane to a higher  $h$  with a decreasing void ratio. So, they can capture the increase in air-entry value well with a decreasing void ratio. However, the predicted adsorption and desorption rates remain unchanged, inconsistent with the previous experimental results (Romero, 1999; Romero et al., 1999). As illustrated in Figure 1a, Equation 2 cannot give good fitting at different densities, mainly because it cannot capture the increase in the desorption rate. The performance of Equation 3 is not shown in the figure because of the similar capabilities of Equations 2 and 3. It should be highlighted that the adsorption/desorption rate can greatly affect the performance of slopes and many engineering structures within unsaturated soils. For instance, Rahimi

et al. (2010) investigated the influence of the adsorption/desorption rate on slope stability during rainfall. They found that the safety factor for the slope depends on the soil's adsorption/desorption rate of the soil as well as the slope's moisture condition prior to rainfall. For an initially relatively dry slope, the factor of safety decreases more rapidly during rainfall if the soil has a higher adsorption/desorption rate. In contrast, for an initially relatively wet slope, the factor of safety decreases more slowly during rainfall under the same conditions. Therefore, incorporating changes in the adsorption/desorption rate into engineering analyses can improve their accuracy, with the potential to enhance construction safety and reduce costs.

On the other hand, some models have been proposed for the relative hydraulic conductivity curve. These models usually derive the relative hydraulic conductivity curve from the water retention curve since they are both related to the pore size distribution. Method by Mualem (1976) has been widely used, which suggests the following equation when Equation 1 is used to model the water retention curve with the constraint of  $m = 1 - 1/n$ :

$$k_r(S_e) = S_e^l \left[ 1 - (1 - S_e^{1/m})^m \right]^2 \quad (4)$$

where  $S_e$  is the effective degree of saturation defined as  $(S_r - S_{rr}) / (1 - S_{rr})$ .  $S_{rr}$  is the residual degree of saturation, and  $l$  is assumed to be 0.5 based on the results of statistical analysis of 45 types of soil. Equation 4 is widely used to predict the relative hydraulic conductivity. As can be seen from this equation, parameter  $m$  obtained by Equation 2 or Equation 3 is constant, so the value of  $k_r$  keeps constant with varying soil density, as illustrated by the model predictions in Figure 1b. Some similar models have been developed (Assouline, 2006; Cai et al., 2014; Hu et al., 2013, 2015; Schaap & Leij, 2000). In addition, some researchers studied  $k_r$  from the perspective of fractal theory (Chen et al., 2023; Ghanbarian et al., 2017; Rad et al., 2020) or pedotransfer functions (Weynants et al., 2009; Zhang et al., 2022). However, as far as the authors are aware, all of the existing models predict that the relationship between  $k_r$  and  $S_e$  is density-independent. They cannot simulate the experimentally observed density-dependency of  $k_r$  (Nemes et al., 2015). Due to this limitation, the predicted hydraulic conductivity may be either overestimated or underestimated, affecting the accuracy of engineering analysis. For example, in the slope stability analysis, an underestimation of  $k_r$  may result in an underestimate of rainfall infiltration and an overestimation of slope stability, leading to unsafe design.

The above review shows some obvious limitations in the existing models for unsaturated soil's hydraulic properties. More studies are needed to model the influence of soil density on the adsorption/desorption rates and the relationship between  $k_r$  and  $S_e$ . All of them are important aspects of hydraulic properties and play important roles in the transient seepage analysis, the management of underground water resources and the analysis of slopes and infrastructures, as explained above. To address these problems, this study proposed a new and simple method to describe the evolution of pore size distribution upon soil deformation. Unlike the equation of Hu et al. (2013), for a given pore, the ratio of its initial and final sizes is considered a function of not only the decrement in void ratio but also the initial size. Based on this equation, a new and simple model for the water retention curve was derived. A model for the relative hydraulic conductivity curve was also developed by incorporating the pore size distribution evolution and tortuosity increase upon soil deformation. To validate the new equations, test data from several soils with distinct properties were used.

## 2. New Equations for Density-Dependent Pore Size Distribution and Hydraulic Properties

### 2.1. Evolution of Pore Size Distribution Under Soil Deformation

The pore size distribution of soil is often described using a pore size density function in the semi-log scale  $f(\ln r)$ . The corresponding integral gives the cumulative pore volume function. Figure 2 shows the pore size density function and cumulative pore volume of Kyoto clay, as an example, obtained from MIP tests. Under soil deformation, the pore size distribution undergoes evolution, and the pore size reduces, as shown in Figure 2a. Similar to Hu et al. (2013), this study describes the reduction of pore size using a shifting factor  $\chi_i^j$ , which is defined as the ratio of the pore radius at the initial state  $r_0^j$  and the pore radii after soil deformation  $r_i^j$ :

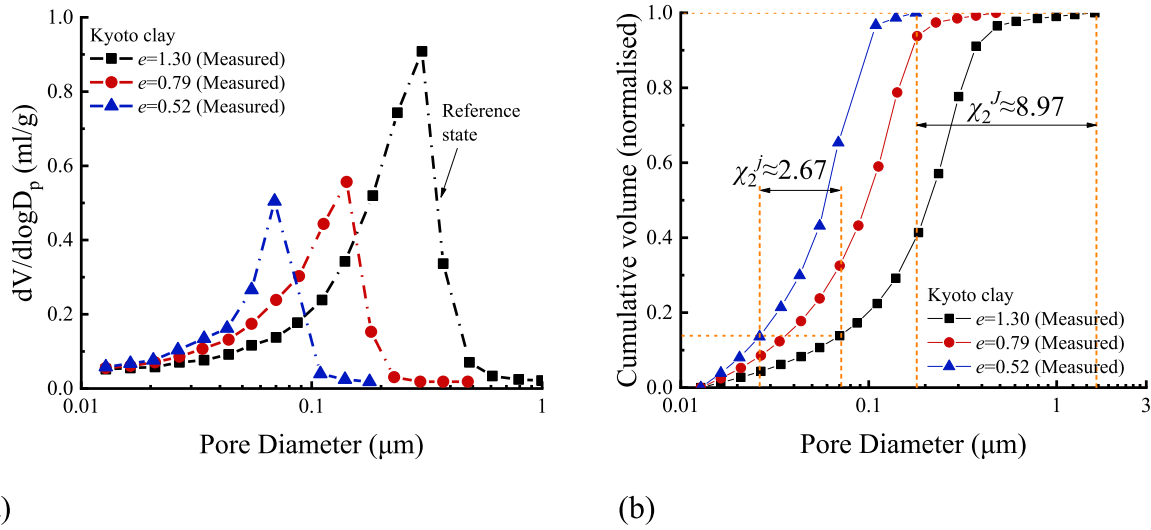


**Figure 2.** Non-uniform variation in pore size distribution and corresponding normalized integral curve of Kyoto clay under loading: (a) pore size distribution and prediction of the modified model; (b) corresponding normalized cumulative curve of panel (a) (data from Tanaka et al. (2003)).

$$\chi_i^j = \frac{r_0^j}{r_i^j} \quad (5)$$

where the superscript  $j$  represents pore  $j$ , and the subscripts 0 and  $i$  denote the initial state or a reference state and deformed state  $i$ . According to this equation, the pore size distribution at the deformed state  $i$  can be linked to the pore size distribution at the initial state as follows:

$$f_i(\ln r) = \eta_i f_0(\ln(r\chi_i^j)) = \eta_i f_0(\ln r + \ln \chi_i^j) \quad (6)$$

where  $f_0$  is the initial pore size distribution function,  $f_i$  is the pore size distribution function at  $i$ th deformed state, and  $\eta_i$  is the ratio of total pore volumes at the deformed state  $i$  and initial state.

It should be pointed out that Hu et al. (2013) assumed that from the initial state to the deformed state  $i$ ,  $\chi_i^j$  is independent of the initial pore size and takes the same value for all pores. As a consequence, the predicted adsorption and desorption rates remain unchanged. This prediction is inconsistent with the previous experimental results (Romero, 1999), as elaborated in the introduction. To address this problem, the current study investigated the characteristics of  $\chi_i^j$  based on experimental results in Figure 2(b). During the loading process, the pore size reduces substantially, and the degree of reduction (i.e., the value of  $\chi_i^j$ ) is not constant. A relatively larger pore  $J$  and a relatively smaller pore  $j$  are selected for better illustration. Pore size distribution at a void ratio of 1.30 is considered the initial state, and pore size distribution at a void ratio of 0.52 is denoted as the second deformed state. It is clear that  $\chi_2^J$  is much larger than  $\chi_2^j$ , meaning that the larger pore has a higher  $\chi_i^j$  value. To simulate the dependency of  $\chi_i^j$  on pore size, Equation 7 is proposed:

$$\chi_i^j = \left( \frac{r_0^j}{r_{ref}^j} \right)^{\beta_i^j} \quad (7)$$

where  $r_{ref}$  is a reference pore radius to make the right-hand side of Equation 7 dimensionless. In the current study, a small value is selected for  $r_{ref}$  to ensure that the ratio  $r_0^j/r_{ref}^j$  is often above 1. The selected  $r_{ref}$  value corresponds to the pressure head of  $10^7$  cm, where the pore diameter predicted by the Young-Laplace equation is comparable to the diameter of water molecules (Fredlund & Xing, 1994). The parameter  $\beta_i^j$  is a non-negative parameter. Consequently, this equation can predict the trend that the value of  $\chi_i^j$  is larger when the initial pore size is larger.

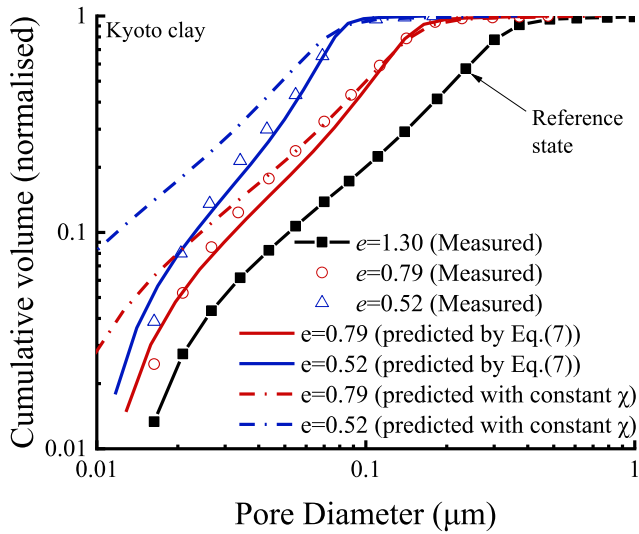


**Figure 3.** Normalized cumulative pore volume of Kyoto clay: comparisons of experimental data (Tanaka et al., 2003), prediction by the new model, and prediction by the Hu et al. (2013) model.

It is interesting to compare Equation 7 and the method of Hu et al. (2013). The predicted pore size distributions are compared with test results in Figure 3. Both methods considered the reduction of pore size under deformation. The method of Hu et al. (2013) assumes that  $\chi_i^j$  is independent of the initial pore size and takes the same value for all pores when the soil is compressed from one void ratio to another one. Hence, their method predicts a parallel shifting of pore size distribution in the figure with  $r$  in the logarithm scale. In contrast, the newly proposed Equation 7 predicts a larger  $\chi_i^j$  value when the initial pore size is larger. Hence, this equation can well capture the pore size reduction for not only relatively larger pores but also relatively smaller pores.

Based on the results of the above analysis, a schematic diagram of the modified model for the pore size distribution evolution is shown in Figure 4. According to Equation 7, the value of  $\chi_i^j$  is larger when the initial pore size is larger, so the initial and final pore size distributions in the  $f$ - $\ln(r)$  plane are not parallel. Moreover, it is reasonable to expect that when  $\Delta e$  is larger, the reduction of pore size becomes more significant, and hence  $\chi_i^j$  and  $\beta_i^j$  increase. Before quantifying the relationship between  $\beta_i^j$  and  $\Delta e$ , it is interesting to obtain the relationship between  $\beta_i^j$  and pore radii in the following form based on Equations 5 and 7:

$$1 - \beta_i^j = \frac{\ln(r_i^j/r_{ref})}{\ln(r_0^j/r_{ref})} \quad (8)$$

Taking logarithms on both sides of Equation 8, Equation 9 can be obtained:

$$\ln(1 - \beta_i^j) = \ln(\ln(r_i^j/r_{ref})) - \ln(\ln(r_0^j/r_{ref})) \quad (9)$$

The right-hand side of Equation 9 is governed by the reduction of  $\ln(\ln(r/r_{ref}))$ . Under soil deformation, pore size and void ratio reduce simultaneously, and the term  $\ln(\ln(r/r_{ref}))$  may have a strong correlation with void ratio  $e$ .

Figure 5 shows a typical result by analyzing the MIP test data of kaolin clay (Jia et al., 2022). In this figure,  $D_{10}$  represents the corresponding pore diameter when the percentage of intruded mercury is 10% of the total pore volume. The other terms ( $D_{30}$ ,  $D_{50}$ ,  $D_{70}$  and  $D_{90}$ ) have a similar definition to  $D_{10}$ . It can be seen that for each term, under compression, a linear relationship between  $\ln(\ln(r/r_{ref}))$  and  $e$  exists. A linear function is proposed to model their relationship:  $\ln(\ln(r^j/r_{ref})) = b^j e + k^j$ , where  $b^j$  and  $k^j$  are two model parameters. By considering the initial and deformed states, this linear equation suggests the following equation:

$$\ln(\ln(r_i^j/r_{ref})) - \ln(\ln(r_0^j/r_{ref})) = -b^j(e_0 - e_i) \quad (10)$$

where  $e_0$  and  $e_i$  are the void ratios in the initial state and deformed state, respectively, and  $b^j$  is dependent on the slope of the fitting curve in Figure 5. Equation 10 gives a semi-empirical relationship between the void ratio and pore radius based on experimental evidence.

Based on Equations 9 and 10, the relationship between  $\beta_i^j$  and  $\Delta e (=e_0 - e_i)$  can be expressed as follows:

$$\beta_i^j = 1 - \exp[-b^j(e_0 - e_i)] \quad (11)$$

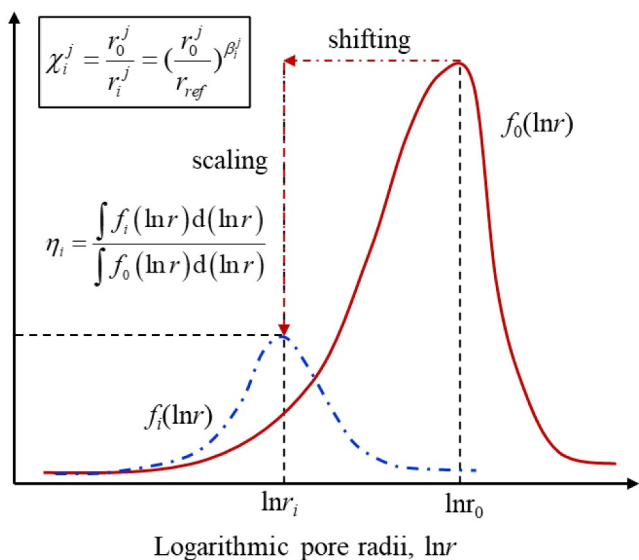


**Figure 4.** Conceptual model considering non-uniform evolution of pore size distribution under deformation (solid line: initial/reference state; dashed line: deformed state).

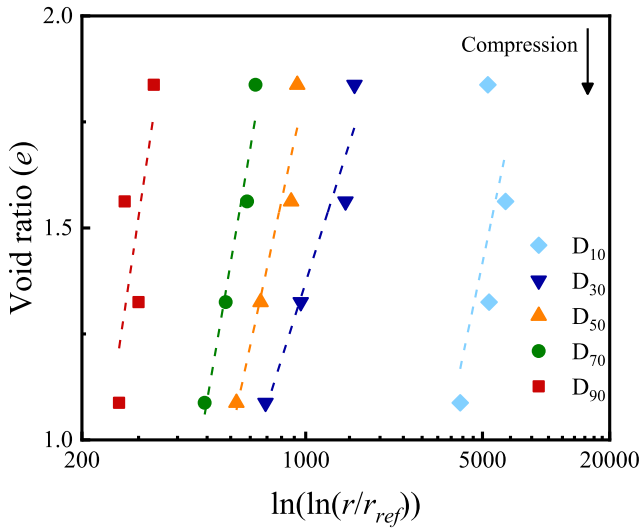


**Figure 5.** The linear relationship between  $\ln(\ln(r/r_{ref}))$  and void ratio ( $e$ ) of Kaolin clay (data from Jia et al. (2022)) during the compression process.

Equation 11 successfully correlates  $\beta_i^j$  with the change in void ratio using a simple form. In addition, the slopes of the fitting curves for different terms ( $D_{10}$ ,  $D_{30}$ ,  $D_{50}$ ,  $D_{70}$  and  $D_{90}$ ) in Figure 5 are almost the same. This means that  $b^j$  and  $\beta_i^j$  can be assumed independent of the initial pore size based on Equations 10 and 11. From the initial state to the deformed state  $i$ , an identical value can be used for all pores. So,  $\beta_i^j$  is simplified as  $\beta_i$  in the following discussion, affected by the constant  $b$  value and the change in void ratio. Once the soil type is determined, parameter  $b$  can be obtained by MIP test results and it is then used to determine  $\beta_i$ . According to Equations 6, 7, and 11, the pore size distribution function  $f_i(\ln r)$  of the deformed state in Figure 4 can be obtained as

$$f_i(\ln r) = \eta_i f_0 \left( \ln \left[ r \left( \frac{r}{r_{ref}} \right)^{\beta_i} \right] \right) = \eta_i f_0 \left( \ln \left( \frac{r^{2-\exp[b(e_0-e_i)]}}{r_{ref}^{1-\exp[b(e_0-e_i)]}} \right) \right) \quad (12)$$

Equation 12 describes the evolution of pore size distribution under soil deformation quantitatively. The shifting factor is a function of initial pore radius and void ratio variation, which can give a better description of pore shifting during deformation. Compared with the previous model (Hu et al., 2013), the conceptual model can better capture the experimental results. This new equation is applied to model the water retention curve and relative hydraulic conductivity of unsaturated soils in the following sections.

## 2.2. Water Retention Model Considering Density Effects on Air-Entry Value and Desorption/Adsorption Rate

The water retention capacity of unsaturated soil is closely related to its pore size distribution. Larger pores are assumed to release water first during the drying process, followed by smaller pores. Therefore, the change in volumetric water content can be determined from the pore density function:

$$d\theta = f(\ln r) d(\ln r) \quad (13)$$

Moreover, for a given pore in unsaturated soil, the relationship between its lowest achievable and pore radius  $r$  follows the Young-Laplace equation:

$$h = \frac{2T_s \cos \alpha^*}{r\gamma_w} \quad (14)$$

where  $T_s$  is the surface tension of water,  $\alpha^*$  is the contact angle, and  $\gamma_w$  is the specific weight of water. Consequently, the value of  $r_{ref}$  equals 0.146 nm ( $T = 20^\circ\text{C}$ ,  $\alpha^* = 0^\circ$ ) where the value of  $T_s$  equals to 72.8 mN/m. During the drying process, this pore is saturated with water when the pressure head is still above this critical value, and water desorption of this pore occurs when the pressure head reaches this critical value.

Based on Equations 13 and 14,  $d\theta$  can also be related to pressure head change:

$$d\theta = f \left( \ln \frac{C}{h} \right) d \left( \ln \frac{C}{h} \right) \quad (15)$$

where  $C = 2T_s \cos \alpha^* / \gamma_w$ . The integral of Equation 15 can be expressed as Equation 16, assuming that  $\theta = \theta_r$ , and adsorption rather than capillary effects dominate water retention behavior, when  $h$  becomes very large:

$$\theta = \int_{\infty}^h f \left( \ln \frac{C}{h} \right) d \left( \ln \frac{C}{h} \right) + \theta_r = \int_h^{\infty} f \left( \ln \frac{C}{h} \right) \frac{1}{h} dh + \theta_r \quad (16)$$

where  $h$  is a dummy variable of integral representing pressure head. To make the expression of Equation 16 simpler, a new function is defined:  $g(h) = f(\ln \frac{C}{h}) \frac{1}{h}$ .  $g(h)$  can be considered as another form of pore size distribution, which is written as a function of pressure head. By substituting this function into Equation 16, it is obtained that

$$\theta = \int_h^\infty g(h) dh + \theta_r \quad (17)$$

It should be noted that various forms of water retention curve are used in the literature, with the soil moisture condition described by the gravimetric water content, volumetric water content, degree of saturation or effective degree of saturation. In the current study, the effective degree of saturation is used because Equation 4 models the relative hydraulic conductivity as a function of  $S_e$ . It is more convenient to consistently use  $S_e$  in the modeling of water retention curve and relative hydraulic conductivity curve.  $S_e$  is a normalized form of volumetric water content and can be written as

$$S_e = \frac{\theta - \theta_r}{\theta_{sat} - \theta_r} \quad (18)$$

where  $\theta_{sat}$  and  $\theta_r$  are the saturated and residual volumetric water contents, respectively.

Based on Equations 17 and 18, it is obtained that

$$S_e = \frac{\int_h^\infty g(h) dh}{\int_0^\infty g(h) dh} \quad (19)$$

Based on the above analysis, the basic relationship between pore size distribution and water retention curve has been established in Equation 19. The influence of soil density on pore size distribution has been modeled using Equation 12. Hence, the evolution of water retention curve under soil deformation can be predicted based on these two equations. This method can be used for different water retention models, which implicitly assume a specific type of pore size distribution. This study uses the VG model (van Genuchten, 1980) as an example. The corresponding initial pore size distribution can be expressed as

$$f_0(\ln r) = -(\theta_{sat} - \theta_r) \frac{\partial S_e}{\partial h} \frac{C}{r} \quad (20)$$

Based on Equation 1, Equation 20 can be rewritten as

$$f_0(\ln r) = (\theta_{sat} - \theta_r) mn \left[ 1 + \left( \frac{\alpha C}{r} \right)^n \right]^{-m-1} \left( \frac{\alpha C}{r} \right)^n \quad (21)$$

In Equation 21, the term  $\theta_{sat} - \theta_r$  can be rewritten as  $\frac{e_0 - w_r G_s}{1 + e_0}$ , where  $w_r$  is the residual gravimetric water content, which is assumed to be independent of soil density.  $G_s$  is the specific gravity. Based on Equations 12 and 21, the pore size distribution function of soils in the deformed state can be expressed as

$$f_i(\ln r) = \eta_i f_0(\ln(r\chi_i)) = \eta_i \left( \frac{e_0 - w_r G_s}{1 + e_0} \right) mn \left[ 1 + \left( \frac{\alpha C^{\beta_i+1} r_{eig}^{\beta_i}}{C^{\beta_i} r^{\beta_i+1}} \right)^n \right]^{-m-1} \left( \frac{\alpha C^{\beta_i+1} r_{eig}^{\beta_i}}{C^{\beta_i} r^{\beta_i+1}} \right)^n \quad (22)$$

Based on Equation 14, the pore size distribution in the form of the pressure head at a deformed state can be expressed as

$$g(h) = -\eta_i \left( \frac{e_0 - w_r G_s}{1 + e_0} \right) mn \left[ 1 + \left( \frac{\alpha}{h_{ref}^{\beta_i}} h^{\beta_i+1} \right)^n \right]^{-m-1} \left( \frac{\alpha}{h_{ref}^{\beta_i}} h^{\beta_i+1} \right)^{n-1} \left( \frac{\alpha}{h_{ref}^{\beta_i}} h^{\beta_i} \right) \quad (23)$$

Based on Equations 20 and 23, the water retention model can be obtained

$$S_e = \frac{\int_h^\infty g_i(h) dh}{\int_0^\infty g_i(h) dh} = \frac{\left[1 + \left(\frac{\alpha}{h_{ref}^{\beta_i}} h^{\beta_i+1}\right)^n\right]^{-m} \Big|_h^\infty}{\left[1 + \left(\frac{\alpha}{h_{ref}^{\beta_i}} h^{\beta_i+1}\right)^n\right]^{-m} \Big|_0^\infty} \quad (24)$$

On the right-hand side of this equation, the integral of the denominator equals  $-1$ . By substituting Equation 11 into Equation 24, the final equation of the water retention curve based on the modified evolution model of pore size distribution can be expressed as

$$S_e = \left[1 + \left(\frac{\alpha}{h_{ref}^{1-\exp[b(e_0-e_i)]}} h^{2-\exp[b(e_0-e_i)]}\right)^n\right]^{-m}, h_{ref} = 10^7 \text{ cm} \quad (25)$$

Equation 25 suggests a density-dependent water retention model, where one new parameter (i.e.,  $b$ ) is added compared with the VG model. The present model can smoothly reduce to the VG model when the variation of the void ratio is zero.

It is interesting to compare the present model, the model proposed by Gallipoli et al. (2003), and the one proposed by Hu et al. (2013). From the perspective of methodology, Gallipoli et al. (2003) gave a semi-empirical function between air-entry value and void ratio based on experimental results. Hu et al. (2013) developed the model for pore size distribution evolution from the microscopic scale, assuming that the shifting factor was a constant value under the given deformation, and then derived a water retention model. The present model is also established from the perspective of microscopic analysis, but the description of pore size distribution evolution is more reasonable, as illustrated above. From the perspective of model capability, the pore size distribution evolution is simplified in the two existing models (see Figure 3), so Equations 2 and 3 can only predict air-entry value increase under deformation. However, in the present modified model, the ratio between initial and final pore sizes is considered a function of the initial pore size. Consequently, the new model has the characteristics that the changes in both air-entry value and adsorption/desorption rate upon soil deformation can be predicted, which is more consistent with experimental results, as shown later.

### 2.3. Relative Hydraulic Conductivity Model Considering the Influence of Soil Density

The hydraulic conductivity  $k_u$  of unsaturated soil can be expressed as the product of saturated hydraulic conductivity  $k_{sat}$  and relative hydraulic conductivity  $k_r$ :

$$k_u = k_{sat} \cdot k_r \quad (26)$$

where  $k_{sat}$  can be readily measured, and its dependency on soil porosity can be predicted by the Kozeny-Carman model (Carman, 1937) or other well-established models. Measuring  $k_r$  is challenging because unsaturated soil testing is complicated and time-consuming, so a reliable prediction model is desired. In this study, the method of Mualem (1976) is modified to model  $k_r$  by considering the evolution of soil pore size distribution upon deformation.

Mualem (1976) considered a slab with a thickness of  $\Delta x$  with two assumptions regarding water flow between the two surfaces of the slab: (a) the two surfaces are connected by a series of circular flow channels, each of which consists of two connected capillary tubes, and the tubes' lengths are proportional to their radii; (b) there is no bypass flow. It was also assumed that unsaturated soil is a homogeneous material, and the areal porosity of each cross-section is identical to the volumetric porosity. On the surfaces of the slab, the pore area distribution can be described using  $f(\ln r)$ . The area of pores with size from  $\ln r$  to  $(\ln r + d \ln r)$  is therefore equal to  $f(\ln r)d(\ln r)$  based on Equation 13. Therefore, the encounter probability of two pores on the two surfaces of the slab, with pore radii of  $\ln r$  and  $\ln \rho$  as well as radii increment of  $d(\ln r)$  and  $d(\ln \rho)$ , equals  $f(\ln r)d(\ln r)f(\ln \rho)d(\ln \rho)$ . The hydraulic conductivity varies as the product of the two pores' radii, that is,  $r\rho$ . Moreover, Mualem (1976) multiplied this probability with a correlation factor  $G$  and a tortuosity factor  $T$ , which were introduced to better consider the correlation between pores (i.e., the pores on the two surfaces of the slab are not connected randomly) and

tortuosity of pore channels formed by two pores. Based on these considerations, Mualem (1976) predicted the water flow in the slab under unsaturated conditions. The incremental form of relative hydraulic conductivity follows

$$dk_r(\ln r, \ln \rho) = \frac{T(\ln R, \ln r, \ln \rho) G(\ln R, \ln r, \ln \rho) r \rho f(\ln r) f(\ln \rho) d(\ln r) d(\ln \rho)}{\int_{\ln r_{\min}}^{\ln r_{\max}} \int_{\ln r_{\min}}^{\ln r_{\max}} T(\ln r_{\max}, \ln r, \ln \rho) G(\ln r_{\max}, \ln r, \ln \rho) r \rho f(\ln r) f(\ln \rho) d(\ln r) d(\ln \rho)} \quad (27)$$

where  $R$  is the radius of the largest pore filled with water in an unsaturated state that corresponds to a pressure head  $h$  following Equation 17.  $r_{\min}$  and  $r_{\max}$  are the minimum and maximum pore radius in soil, corresponding to the pressure heads of  $h_{\max}$  and 0, respectively. Based on Equation 27, the relative hydraulic conductivity can be expressed as Equation 28:

$$k_r(R) = \frac{\int_{\ln r_{\min}}^{\ln R} \int_{\ln r_{\min}}^{\ln R} T(\ln R, \ln r, \ln \rho) G(\ln R, \ln r, \ln \rho) r \rho f(\ln r) f(\ln \rho) d(\ln r) d(\ln \rho)}{\int_{\ln r_{\min}}^{\ln r_{\max}} \int_{\ln r_{\min}}^{\ln r_{\max}} T(\ln r_{\max}, \ln r, \ln \rho) G(\ln r_{\max}, \ln r, \ln \rho) r \rho f(\ln r) f(\ln \rho) d(\ln r) d(\ln \rho)} \quad (28)$$

The denominator on the right-hand side of Equation 28 equals the saturated hydraulic conductivity, while the numerator is the hydraulic conductivity at an unsaturated state. The moisture condition can impact the value of the numerator. In an unsaturated state, pores with radii larger than  $R$  are not filled with water. Thus, a reduced amount of water-filled pores diminishes the effective pore channel formation for water flow, decreasing hydraulic conductivity. Based on a further assumption that tortuosity and correlation factors are power functions of  $S_e$  (Mualem, 1976), Equation 28 can be simplified to the following two equivalent forms:

$$k_r(R) = \left[ \frac{\int_{\ln r_{\min}}^{\ln R} r f(\ln r) d(\ln r)}{\int_{\ln r_{\min}}^{\ln r_{\max}} r f(\ln r) d(\ln r)} \right]^2 S_e^l \quad (29a)$$

$$k_r(S_e) = \left[ \frac{\int_0^{S_e} h^{-1} d(S_e)}{\int_0^1 h^{-1} d(S_e)} \right]^2 S_e^l \quad (29b)$$

where  $l$ , in Equation 29 is an index related to the tortuosity of the flow path and the correlation between pores. For the two terms on the right-hand side of Equation 29, their physical meaning and evolution upon soil deformation warrant attention, as discussed below.

First of all,  $\int_{\ln r_{\min}}^{\ln R} r f(\ln r) d(\ln r)$  in the first term considers the influence of the quantity and dimensions of pores filled with water in the unsaturated state, while  $\int_{\ln r_{\min}}^{\ln r_{\max}} r f(\ln r) d(\ln r)$  is the corresponding term at the saturated state. As soil becomes denser, the value of  $\left[ \int_{\ln r_{\min}}^{\ln R} r f(\ln r) d(\ln r) \right]^2$  decreases, which represents the contribution of relatively smaller pores (i.e., from  $r_{\min}$  to  $R$ ) on hydraulic conductivity. Meanwhile, the value of saturated hydraulic conductivity decreases, which can be attributed to the decrease of both relatively smaller and larger pores (i.e., from  $R$  to  $r_{\max}$ ), written as  $\left[ \int_{\ln r_{\min}}^{\ln R} r f(\ln r) d(\ln r) + \int_{\ln R}^{\ln r_{\max}} r f(\ln r) d(\ln r) \right]^2$ . As illustrated above, the radii of larger pores decrease more significantly than that of smaller pores under deformation. Therefore, the decrease in hydraulic conductivity  $\int_{\ln R}^{\ln r_{\max}} r f(\ln r) d(\ln r)$ , due to the relatively larger pores' size reduction, is greater than relatively smaller pores. Consequently, the value of the first term  $\left[ \int_{\ln r_{\min}}^{\ln R} r f(\ln r) d(\ln r) / \int_{\ln r_{\min}}^{\ln r_{\max}} r f(\ln r) d(\ln r) \right]^2$  shows an increasing trend under deformation.

Secondly, the other term  $S_e^l$  represents the quality of the pore channels, which is related to the tortuosity of flow paths. The increase in tortuosity results in a decrease in pore channels' quality and hydraulic conductivity. Furthermore, the tortuosity of flow paths is mainly affected by the change in moisture content and intrinsic tortuosity of pore channels. The former is considered using the term  $S_e^l$ , as proposed by Mualem (1976). For the latter one, experimental data in the literature generally show that the intrinsic tortuosity of pore channels increases with increasing density (Comiti & Renaud, 1989; Wyllie & Gregory, 1955), as illustrated by the example in

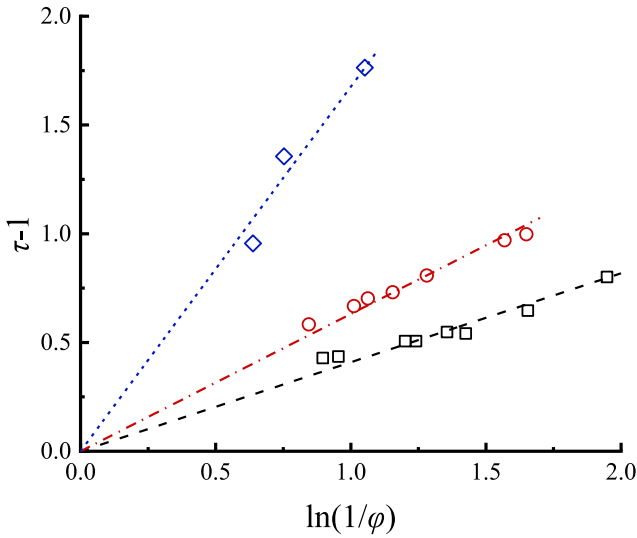


**Figure 6.** Experimental evidence of the relationship between tortuosity factor and porosity of packed bed (Comiti & Renaud, 1989).

Figure 6, where  $\varphi$  denotes porosity. It can be noticed from the experimental results that when soil becomes denser, the increase in tortuosity becomes less significant. To incorporate the influence of density on tortuosity and relative hydraulic conductivity, it is reasonable to consider parameter  $l_t$  as a function of density. In this study, a semi-empirical relationship between the increment of void ratio  $\Delta e$  and  $l_t$  is proposed as

$$l_t = 0.5\sqrt{1 + l \cdot \Delta e} \quad (30)$$

where  $l$  is the parameter related to soil type. The value of  $S_e^l$  shows a decreasing trend upon deformation. Equation 30 can be smoothly reduced to the Mualem (1976) model (i.e.,  $l_t = 0.5$ ) in the absence of deformation.

By substituting Equations 25 and 30 into Equation 29, the relative hydraulic conductivity can be rewritten as

$$k_r = \left[ \frac{\int_0^{S_e} h^{-1} d(S_e)}{\int_0^1 h^{-1} d(S_e)} \right]^2 S_e^{0.5\sqrt{1+l \cdot \Delta e}} \quad (31)$$

It is clear from Equation 31 that  $k_r$  is a function of both  $\Delta e$  and  $S_e$ , unlike previous models (e.g., Equation 4) that do not consider the influence of soil deformation. Based on the newly proposed model, the deformation can change at least the pore size distribution and intrinsic tortuosity of pore channels. On the one hand, the pore size distribution tends toward greater uniformity, thereby enhancing the probability of pore channel formation and increasing  $k_r$ . On the other hand, the increase in intrinsic tortuosity decreases  $k_r$ . These two opposite trends control the variation of  $k_r$  with density. In addition, the relative hydraulic conductivity curve described by Equation 31 does not have a closed-form expression, while numerical integral can be used to calculate  $k_r$  in this study.

### 3. Model Validation

#### 3.1. Calibration Method of Model Parameters

The parameters in the new model for the water retention and relative hydraulic conductivity curves were calibrated simultaneously because this method can significantly improve the model prediction, as demonstrated by Weynants et al. (2009) and Zhang et al. (2022). For each soil, two water retention curves with different initial densities were used to obtain the parameters  $\alpha$ ,  $n$ ,  $m$ , and  $b$  in Equation 25. Then, these four parameters were adjusted using one  $k_r$ - $S_e$  curve. After parameters  $\alpha$ ,  $n$ ,  $m$ , and  $b$  were determined, the additional parameter (i.e.,  $l$ ) was calibrated by another  $k_r$ - $S_e$  curve in Equation 31.

#### 3.2. Test Data for Model Validation

After parameter calibration, the water retention and relative hydraulic conductivity curves can be calculated using Equations 25 and 31. In this section, the new equations are validated using the experimental results of several different soils, for which both the water retention and relative hydraulic conductivity curves were reported. The data utilized were collected from previous experimental studies (e.g., Ciollaro & Comegna, 1988; Romero, 1999) and the data set collected by USDA (Nemes et al., 2015). Table 1 summarizes the value of model parameters for all soils. The new model's performance was also compared with that of existing models. Root mean square error (RMSE) was utilized to evaluate model prediction quality, and the results are summarized in Table 2.

#### 3.3. Comparisons Between the New and Existing Models

Figure 7 shows the water retention curves of Boom clay with three different initial void ratios. With the decrease in void ratio, the air-entry value and desorption rate show an increasing trend. As discussed above, the VG model (i.e., Equation 1) can only predict one curve because it does not consider the density effects. Advanced models (e.g., Equations 2 and 3) can capture the increase in air-entry value but not the change in desorption rate, as illustrated in Figure 1a. To evaluate the performance of the new model, Equation 25 was applied to analyze the

**Table 1**  
Soil Parameters Given by the UNSODA Database (Nemes et al. (2015)) (Marked by \*) and Parameters Newly Calibrated for the Water Retention Curve and Relative Hydraulic Conductivity

Soil	Void ratio ( $e$ )*	Saturated volumetric water content ( $\theta_{sat}$ )*	Residual volumetric water content ( $\theta_r$ )	Saturated hydraulic conductivity ( $k_s$ ) $10^{-6} \text{ m}\cdot\text{s}^{-1}$ *)	$\alpha$	$m$	$n$	$b$	$l$
Masseria Bozza sand	0.68	0.336	0.054	6.3	0.27	0.367	1.54	0.52	944.0
	0.46	0.270	0.115	0.4					
Riedhof silt loam	1.45	0.572	0.078	15.0	0.60	0.286	1.31	0.27	996.3
	1.05	0.491	0.102	4.2					
	0.57	0.371	0.161	0.8					
Berlin fine sand	0.71	0.392	0.019	24.8	0.19	0.251	7.43	0.14	638.0
	0.62	0.320	0.023	4.6					
Berlin medium sand	0.75	0.315	0.009	115.7	0.94	0.483	1.93	0.42	0.1
	0.66	0.388	0.015	80.1					
	0.58	0.357	0.013	23.1					
Berlin coarse sand	0.60	0.362	0.0013	231.5	2.83	0.072	8.8	0.63	39.2
	0.42	0.361	0.009	29.1					
Unconsolidated sand	0.80	0.445	0.042	1,216.2	2.13	0.166	22.61	0.19	3.0
	0.78	0.439	0.045	1,111.5					
	0.74	0.424	0.043	891.1					
Ferdinando loam	0.94	0.426	0.148	1.5	0.13	0.359	1.56	0.52	977.8
	0.81	0.401	0.163	2.7					
Sandy loam	0.56	0.320	0	4.2	0.41	0.117	1.09	0.36	0
	0.42	0.280	0	2.1					

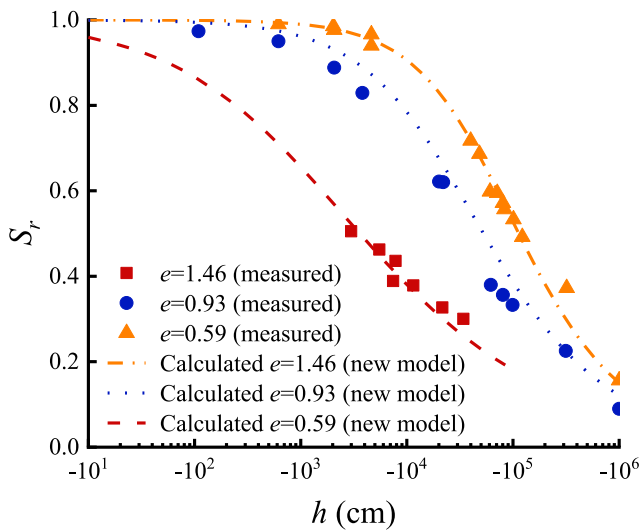
experimental results. The water retention curves were calculated and shown in Figure 7 using the parameter values in Table 1. It can be seen that the new model can capture the increasing trend of air-entry value and desorption rate under deformation. It suggests that it is reasonable and necessary to incorporate the non-parallel shifting of pore size distribution under deformation.

Figure 8a shows the measured drying water retention curves for Masseria Bozza sand. It can be seen from the measured data that the air-entry value of this soil increases with the decrease in void ratio while the desorption rate remains almost constant. Hence, both the new and Gallipoli et al. (2003) models can capture the water retention curve well at various void ratios. In contrast, the VG model can only predict one curve at various void ratios. On the other hand, Figure 8b depicts the relative hydraulic conductivity curves of the same soil. The test data shows an increase in  $k_r$  when deformation occurs under a constant  $S_e$ . Only the new model can capture this trend.

Figure 9a shows the water retention of Riedhof silt loam, which is a fine-grained soil. There is an increase in air-entry value as well as desorption rate with a decrease in void ratio, even though the latter is less obvious. The relative hydraulic conductivity in Figure 9b decreases with increasing density. The results calculated using the new model are well-matched with the measured data at a relatively low-pressure head. However, there are some obvious differences when the pressure head is relatively large, likely because the new model does not model the

**Table 2**  
Root Mean Square Error Values for the New Model and Some Representative Existing Models

Soil	Water retention curve			Relative hydraulic conductivity curve		
	New model	Model of van Genuchten (1980)	Model of Hu et al. (2015)	New model	Model of van Genuchten (1980)	Model of Hu et al. (2015)
Masseria Bozza sand	0.027	0.162	0.028	0.504	1.119	1.063
Riedhof silt loam	0.045	0.683	0.046	1.403	1.729	1.750



**Figure 7.** Comparison of measured (Romero, 1999) and calculated water retention curves for Boom clay.

adsorption effects. In addition, similar to the observations in Figure 8, the new model performs better than the existing models.

Based on the above comparisons, it is clear that the new models can better capture the density effects on the water retention and relative hydraulic conductivity curves of unsaturated soils. The conclusion can be equally applicable to other soils. Hence, the following sections focus on the validation of the new model using the test data of different soils (coarse- and fine-grained soils). The comparisons between different models are not shown for conciseness.

### 3.4. Validating the New Model Using Test Data of Coarse-Grained Soils

Figures 10–12 depict the measured and calculated results of three sands. These three soils are from Berlin and have distinct particle size distributions (Nemes et al., 2015). For the water retention curve of two sands (see Figures 10a and 11a), with the increase in density, the air-entry value and desorption rate increase. The model prediction is well-matched with the corresponding measured data. In contrast, the air-entry value and desorption rate of the other sand (see Figure 12a) do not align with the trend predicted by the current model. The discrepancies are likely attributed to experimental

errors, given the difficulty of accurately controlling low pressure head, as well as some special properties of this soil's pore size distribution evolution.

By comparing the results in Figures 10b, 11b, and 12b, the density effects on the relative hydraulic conductivity are distinct for these three sands. The Berlin medium sand showed the lowest sensitivity, followed by Berlin coarse sand and Berlin fine sand. For Berlin fine sand and Berlin coarse sand, the predictions by the new model agree with the test data. However, for Berlin medium sand, the new model overestimates the relative hydraulic conductivity when the degree of saturation is lower than 40%. The overestimation is because when the degree of saturation is low, the adsorption effects would reduce the water flow. The new model of this study does not consider the adsorption effects and tends to overestimate the hydraulic conductivity.

Figure 13 shows the measured and calculated water retention curves and relative hydraulic conductivity curves of another sand. The denser specimen has a larger air-entry value than the looser specimen, while the difference in desorption rate is unclear. The proposed model well captures these observations. On the other hand, the  $k_r$ - $S_e$  relation is not very sensitive to density (see Figure 13b). There is a minor reduction of  $k_r$  with increasing density,

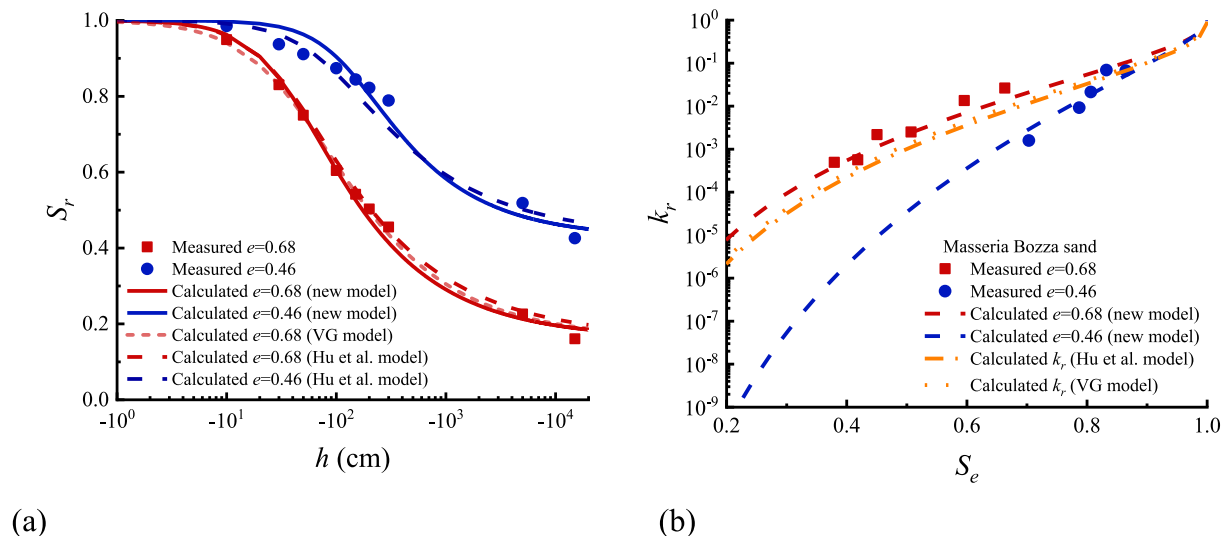


**Figure 8.** Comparison of measured and calculated results for Masseria Bozza sand: (a) water retention curve; (b) relative hydraulic conductivity curve (data from Ciollaro and Comegna (1988)).

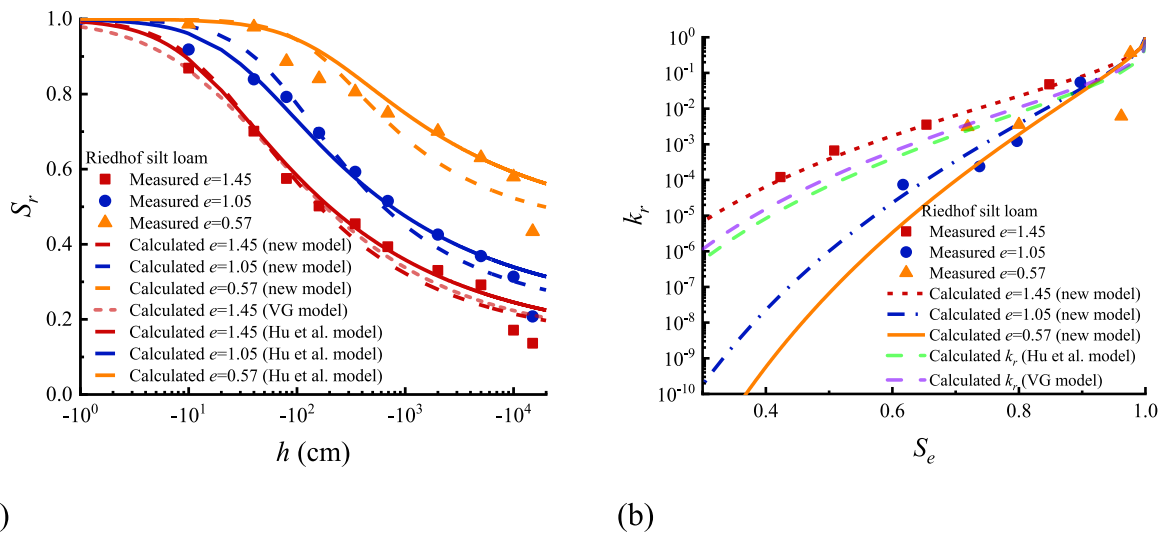


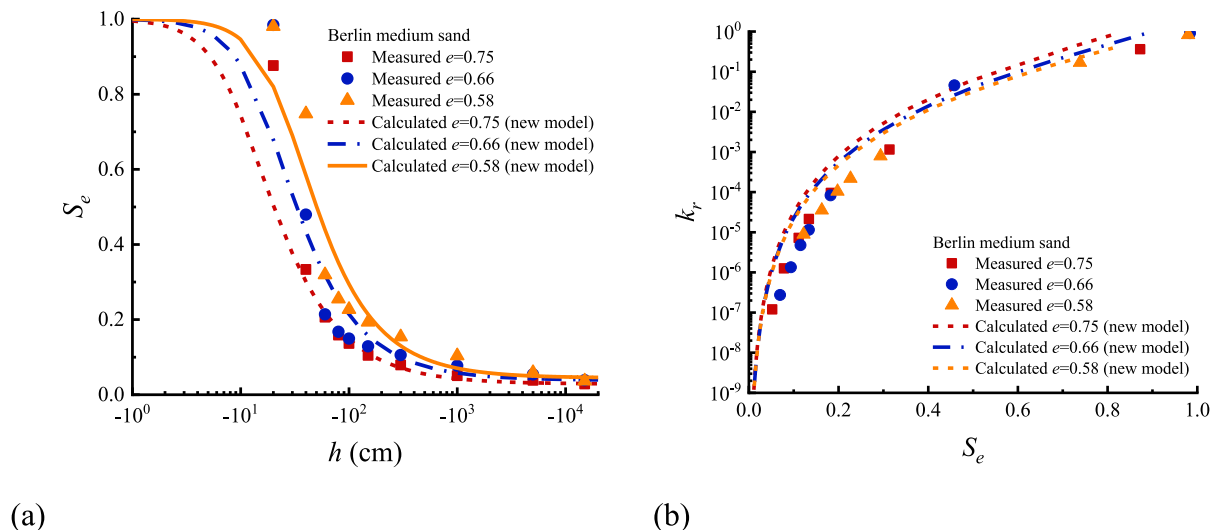
**Figure 9.** Comparison of measured and calculated results for Riedhof silt loam: (a) water retention curve; (b) relative hydraulic conductivity curve (data from Nemes et al. (2015)).

and the new model can capture this slight difference well. When the effective degree of saturation is higher than 0.4, however, the difference between the measured and calculated results is obvious.

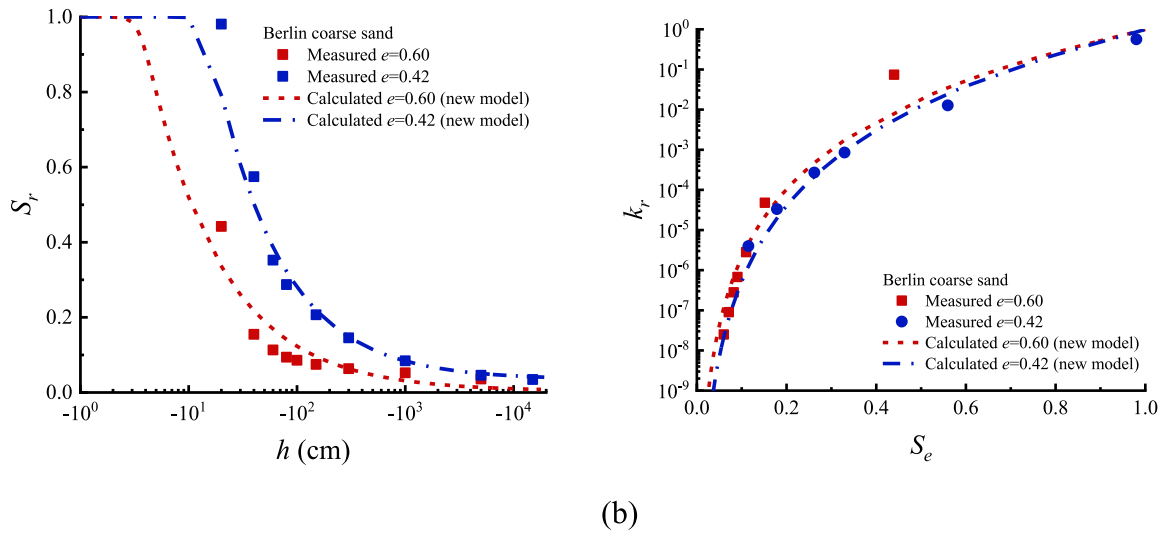
### 3.5. Validating the New Model Using Test Data of Fine-Grained Soils

Figure 14a illustrates the measured and calculated water retention curves of a loam. The denser specimen shows a higher air-entry value and a slightly higher desorption rate than the looser one. The new water retention model agrees well with the air-entry value and the desorption rate. A density-dependency of  $k_r$  is evident and can be captured by the new model, as illustrated in Figure 14b.

Figure 15 shows a sandy loam's water retention and relative hydraulic conductivity curves. The calculated water retention curves show a good agreement with the measured data. For the relative hydraulic conductivity of this soil, it should be highlighted that it shows an increasing trend with the increase in density, different from the trend of other soils (see Figures 8–14). This means that during soil deformation, the value of  $k_r$  either decreases or increases depending on the soil type. The proposed model can explain these two trends because an increase in



**Figure 10.** Comparison of measured and calculated results for Berlin medium sand: (a) water retention curve; (b) relative hydraulic conductivity curve (data from Nemes et al. (2015)).



**Figure 11.** Comparison of measured and calculated results for Berlin coarse sand: (a) water retention curve; (b) relative hydraulic conductivity curve (data from Nemes et al. (2015)).

tortuosity reduces the relative hydraulic conductivity, while the change in pore size distribution increases it. Both mechanisms are considered in the new model.

In addition, the measured and calculated relative hydraulic conductivities in Figure 15 are quite different in this figure. The difference is likely because, according to the data of Ciollaro and Comegna (1988), the measured  $k_u$  at a higher density is slightly larger than that of a smaller one, which is not consistent with the relationship between  $k_u$  and  $e$  shown by other soils analyzed before. This unusual behavior may be partially due to experimental errors and partially because the pore size distribution of this soil does not change as assumed.

#### 4. Conclusions

This study proposed a new equation to describe the pore size distribution evolution under deformation. Based on this, a new water retention equation for unsaturated soils has been developed. The new water retention model can better capture the density effects, describing a higher air-entry value and adsorption/desorption rate in a denser state.

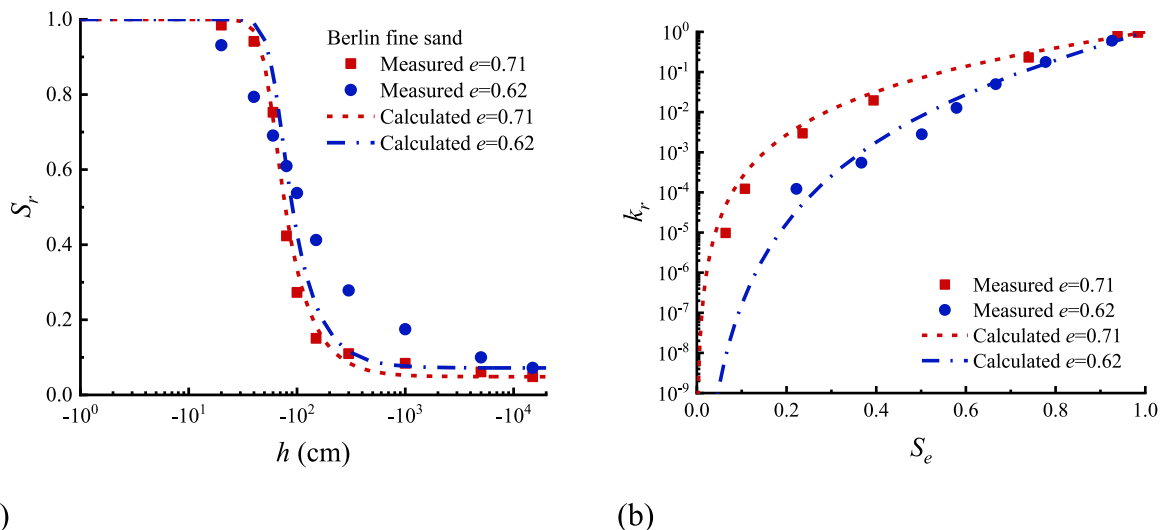


**Figure 12.** Comparison of measured and calculated data for Berlin fine sand: (a) water retention curve; (b) relative hydraulic conductivity curve (data from Nemes et al. (2015)).

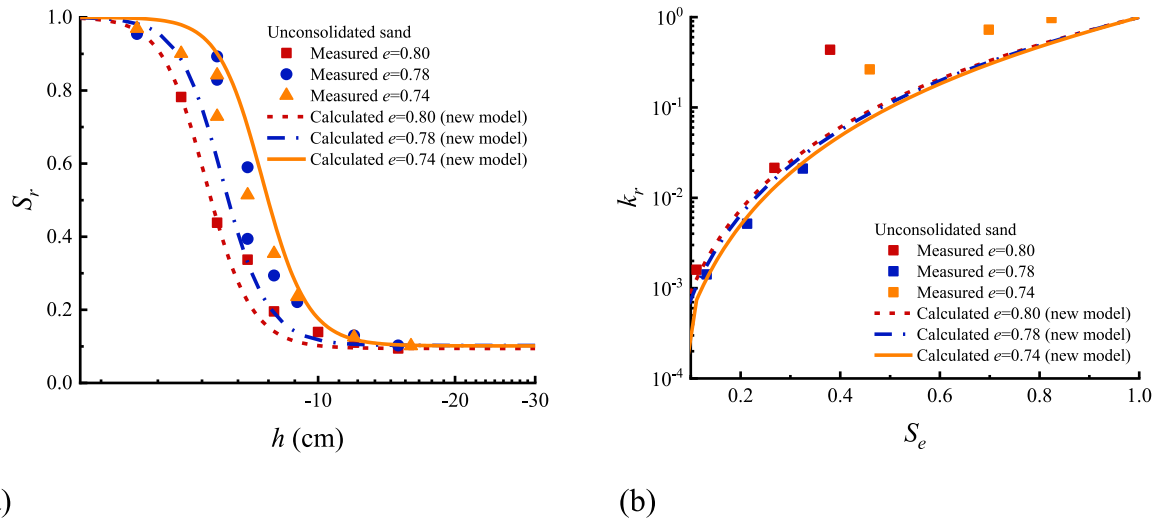


**Figure 13.** Comparison of measured and calculated results for unconsolidated sand: (a) water retention curve; (b) relative hydraulic conductivity curve (data from Laliberte et al. (1966)).

Another new equation was developed to capture the change in relative hydraulic conductivity with increasing density. This model is built on the new water retention model and the fact that higher density results in a larger tortuosity of pore channels. Consequently, the increase in density may have two competing effects on the relative hydraulic conductivity: (a) an increased trend in relative hydraulic conductivity due to a more significant shifting of relatively large pores and (b) a decreasing trend in relative hydraulic conductivity because of degradation in pore channels' quality (high pore tortuosity).

The results of several coarse- and fine-grained soils are used to validate the new models, and good agreements are witnessed in most of them. Compared with previous models, the predictions of modified models are more consistent with experimental results.

Compared to existing models, the new model has addressed two specific problems important for engineering analysis: (a) simulating an increase in not only air-entry value but also adsorption/desorption rate as the soil becomes denser; (b) accounting for the variation of relative permeability  $k_r$  at a given degree of saturation with soil density.

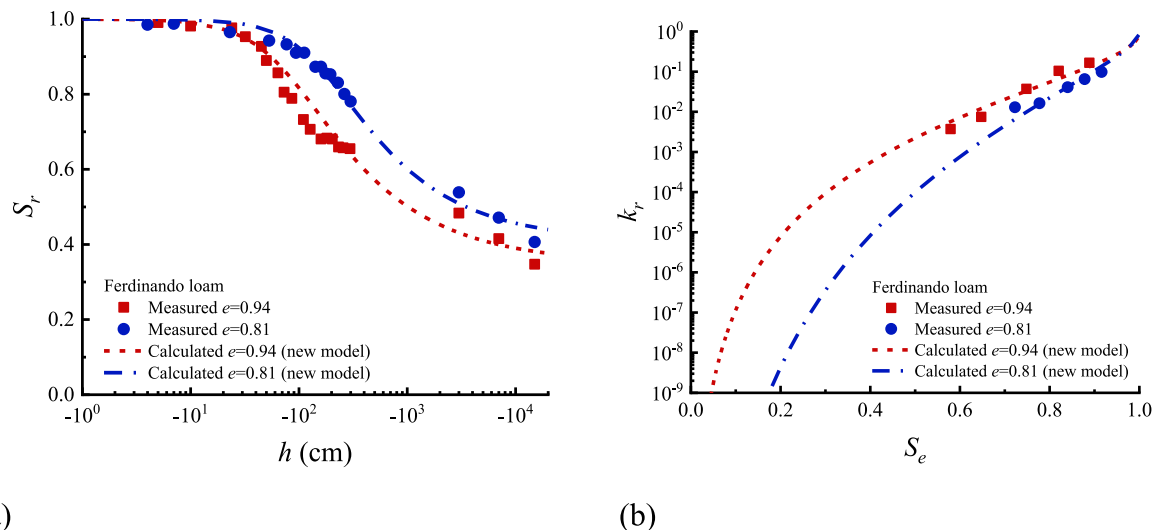


**Figure 14.** Comparison of measured and calculated results for Ferdinando loam: (a) water retention curve; (b) relative hydraulic conductivity curve (data from Nemes et al. (2015)).

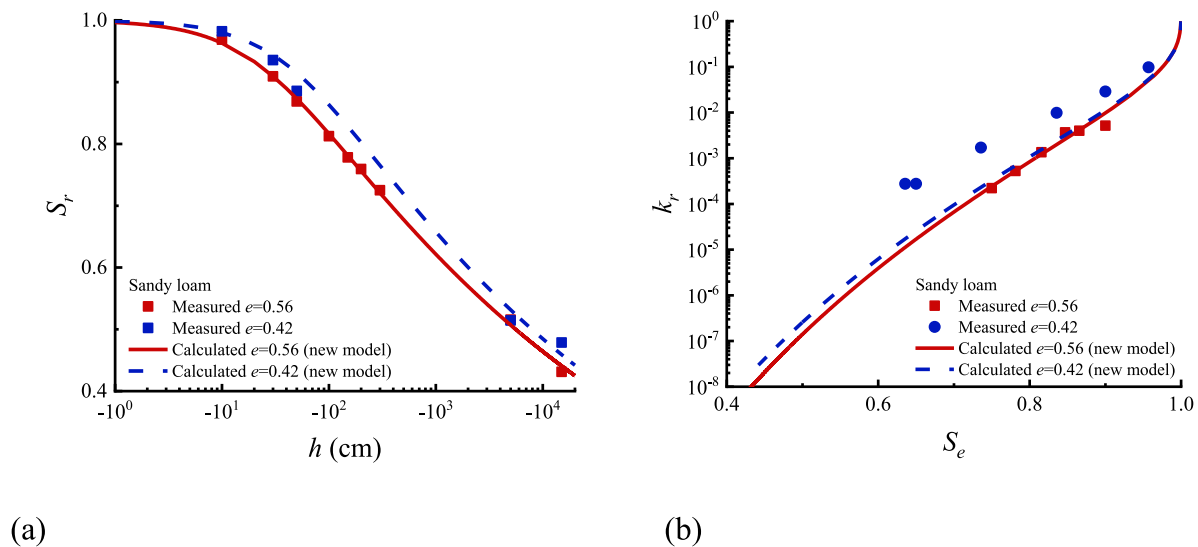


**Figure 15.** Comparison of measured and calculated results for sandy loam: (a) water retention curve; (b) relative hydraulic conductivity curve (data from Ciollaro and Comegna (1988)).

### Data Availability Statement

The water retention curve in Figures 1a and 7 are collected from Chapter 5 Figure 5.9 in Ph.D thesis of Romero (1999), which can be accessed at <https://upcommons.upc.edu/handle/2117/93536>. The MIP test data in Figures 2 and 3 are collected from Figure 4b in the research of Tanaka et al. (2003). The data in Figure 5 are collected and analyzed based on the MIP test data in Figure 10 in the research of Jia et al. (2022). The data in Figure 6 are collected from Figure 4 in the research of Comiti and Renaud (1989). The data in Figures 8–15 can be found in the UNSODA database (Nemes et al., 2015), where the original references of the data in Figures 8, 13, and 15 are given in the captions.

### References

- Assouline, S. (2006). Modeling the relationship between soil bulk density and the hydraulic conductivity function. *Vadose Zone Journal*, 5(2), 697–705. <https://doi.org/10.2136/vzj2005.0084>
- Assouline, S., Tessier, D., & Braund, A. (1998). A conceptual model of the soil water retention curve. *Water Resources Research*, 34(2), 223–231. <https://doi.org/10.1029/97wr03039>
- Bella, G. (2021). Water retention behaviour of tailings in unsaturated conditions. *Geomechanics and Engineering*, 26(2), 117–132. <https://doi.org/10.12989/gae.2021.26.2.117>
- Cai, G. Q., Zhou, A. N., & Sheng, D. C. (2014). Permeability function for unsaturated soils with different initial densities. *Canadian Geotechnical Journal*, 51(12), 1456–1467. <https://doi.org/10.1139/cgj-2013-0410>
- Carman, P. C. (1937). Fluid flow through granular beds. *Chemical Engineering Research and Design*, 75, S32–S48. [https://doi.org/10.1016/S0263-8762\(97\)80003-2](https://doi.org/10.1016/S0263-8762(97)80003-2)
- Chen, K., Wang, C., & Liang, F. Y. (2023). Fractal-based hydraulic model of unsaturated flow in deformable soils considering the evolution of pore size distribution. *Journal of Hydrology*, 620, 129501. <https://doi.org/10.1016/j.jhydrol.2023.129501>
- Ciollaro, G., & Comegna, V. (1988). Spatial variability of soil hydraulic properties of a psammentic paleixeralfs soil of south Italy. *Acta Horticulturae*, 228, 61–72. <https://doi.org/10.17660/ActaHortic.1988.228.5>
- Comiti, J., & Renaud, M. (1989). A new model for determining mean structure parameters of fixed-beds from pressure-drop measurements - Application to beds packed with parallelepipedal particles. *Chemical Engineering Science*, 44(7), 1539–1545. [https://doi.org/10.1016/0009-2509\(89\)80031-4](https://doi.org/10.1016/0009-2509(89)80031-4)
- Fan, Y., Clark, M., Lawrence, D. M., Swenson, S., Band, L. E., Brantley, S. L., et al. (2019). Hillslope hydrology in global change research and earth system modeling. *Water Resources Research*, 55(2), 1737–1772. <https://doi.org/10.1029/2018wr023903>
- Fredlund, D. G., & Rahardjo, H. (1993). *Soil mechanics for unsaturated soils*. John Wiley & Sons.
- Fredlund, D. G., Sheng, D. C., & Zhao, J. D. (2011). Estimation of soil suction from the soil-water characteristic curve. *Canadian Geotechnical Journal*, 48(2), 186–198. <https://doi.org/10.1139/T10-060>
- Fredlund, D. G., & Xing, A. Q. (1994). Equations for the soil-water characteristic curve. *Canadian Geotechnical Journal*, 31(4), 521–532. <https://doi.org/10.1139/t94-061>
- Fu, Y. W., Horton, R., Ren, T. S., & Heitman, J. (2023). An unsaturated hydraulic conductivity model based on the capillary bundle model, the Brooks-Corey model and Waxman-Smits model. *Water Resources Research*, 59(6), e2022WR034186. <https://doi.org/10.1029/2022WR034186>
- Gallipoli, D., Wheeler, S. J., & Karstunen, M. (2003). Modelling the variation of degree of saturation in a deformable unsaturated soil. *Géotechnique*, 53(1), 105–112. <https://doi.org/10.1680/geot.53.1.105.37249>

### Acknowledgments

The authors also would like to thank the Research Grants Council of the HKSAR for providing financial support through Grants N\_PolyU526/23, 15205721 and AoE/E-603/18.

- Ghanbarian, B., Ioannidis, M. A., & Hunt, A. G. (2017). Theoretical insight into the empirical tortuosity-connectivity factor in the water relative permeability model. *Water Resources Research*, 53(12), 10395–10410. <https://doi.org/10.1002/2017wr021753>
- Hu, R., Chen, Y. F., Liu, H. H., & Zhou, C. B. (2013). A water retention curve and unsaturated hydraulic conductivity model for deformable soils: Consideration of the change in pore-size distribution. *Géotechnique*, 63(16), 1389–1405. <https://doi.org/10.1680/geot.12.P.182>
- Hu, R., Chen, Y. F., Liu, H. H., & Zhou, C. B. (2015). A relative permeability model for deformable soils and its impact on coupled unsaturated flow and elasto-plastic deformation processes. *Science China Technological Sciences*, 58(11), 1971–1982. <https://doi.org/10.1007/s11431-015-5948-3>
- Jia, R., Lei, H. Y., Hino, T., & Li, K. (2022). Changes in the permeability and permeability anisotropy of reconstituted clays under one-dimensional compression and the corresponding micromechanisms. *International Journal of Geomechanics*, 22(2), 04021282. [https://doi.org/10.1061/\(ASCE\)Gm.1943-5622.0002260](https://doi.org/10.1061/(ASCE)Gm.1943-5622.0002260)
- Kosugi, K. i. (1994). Three-parameter lognormal distribution model for soil water retention. *Water Resources Research*, 30(4), 891–901. <https://doi.org/10.1029/93wr02931>
- Laliberte, G. E., Corey, A. T., & Brooks, R. H. (1966). *Properties of unsaturated porous media* (Vol. 17). Colorado State University.
- Lee, I. M., Sung, S. G., & Cho, G. C. (2005). Effect of stress state on the unsaturated shear strength of a weathered granite. *Canadian Geotechnical Journal*, 42(2), 624–631. <https://doi.org/10.1139/T04-091>
- Li, P. J., Zha, Y. Y., Zuo, B. X., & Zhang, Y. G. (2023). A family of soil water retention models based on sigmoid functions. *Water Resources Research*, 59(3), e2022WR033160. <https://doi.org/10.1029/2022WR033160>
- Li, X., & Zhang, L. M. (2009). Characterization of dual-structure pore-size distribution of soil. *Canadian Geotechnical Journal*, 46(2), 129–141. <https://doi.org/10.1139/T08-110>
- Moghaddasi, H., Esgandani, G. A., Khoshghalb, A., Shahbodagh-Khan, B., & Khalili, N. (2017). A bounding surface plasticity model for unsaturated soils accounting for the void ratio dependency of the water retention curve. In *Poromechanics VI* (pp. 1061–1068).
- Mualem, Y. (1976). A new model for predicting the hydraulic conductivity of unsaturated porous media. *Water Resources Research*, 12(3), 513–522. <https://doi.org/10.1029/WR012i003p00513>
- Nemes, A., Schaap, M., Leij, F. J., & Wösten, J. H. M. (2015). UNSODA 2.0: Unsaturated Soil Hydraulic Database. Database and program for indirect methods of estimating unsaturated hydraulic properties [Dataset]. *US Salinity Laboratory - ARS - USDA*. <https://doi.org/10.15482/USDA.ADC/1173246>
- Ng, C. W. W., & Pang, Y. W. (2000). Experimental investigations of the soil-water characteristics of a volcanic soil. *Canadian Geotechnical Journal*, 37(6), 1252–1264. <https://doi.org/10.1139/t00-056>
- Ng, C. W. W., & Peprah-Manu, D. (2023). Pore structure effects on the water retention behaviour of a compacted silty sand soil subjected to drying-wetting cycles. *Engineering Geology*, 313, 106963. <https://doi.org/10.1016/j.enggeo.2022.106963>
- Ng, C. W. W., Zhou, C., & Ni, J. J. (2024). *Advanced unsaturated soil mechanics: Theory and applications*. CRC Press.
- Rad, A. M., Ghahraman, B., Mosaedi, A., & Sadegh, M. (2020). A universal model of unsaturated hydraulic conductivity with complementary adsorptive and diffusive process components. *Water Resources Research*, 56(2), e2019WR025884. <https://doi.org/10.1029/2019WR025884>
- Rahimi, A., Rahardjo, H., & Leong, E. C. (2010). Effect of hydraulic properties of soil on rainfall-induced slope failure. *Engineering Geology*, 114(3–4), 135–143. <https://doi.org/10.1016/j.enggeo.2010.04.010>
- Romero, E. (1999). *Characterisation and thermo-hydro-mechanical behaviour of unsaturated Boom clay: An experimental study*. Universitat Politècnica de Catalunya.
- Romero, E., Gens, A., & Lloret, A. (1999). Water permeability, water retention and microstructure of unsaturated compacted Boom clay. *Engineering Geology*, 54(1–2), 117–127. [https://doi.org/10.1016/S0013-7952\(99\)00067-8](https://doi.org/10.1016/S0013-7952(99)00067-8)
- Schaap, M. G., & Leij, F. J. (2000). Improved prediction of unsaturated hydraulic conductivity with the Mualem-van Genuchten model. *Soil Science Society of America Journal*, 64(3), 843–851. <https://doi.org/10.2136/sssaj2000.643843x>
- Sun, W. J., & Sun, D. A. (2012). Coupled modelling of hydro-mechanical behaviour of unsaturated compacted expansive soils. *International Journal for Numerical and Analytical Methods in Geomechanics*, 36(8), 1002–1022. <https://doi.org/10.1002/nag.1036>
- Tanaka, H., Shiwakoti, D. R., Omukai, N., Rito, F., Locat, J., & Tanaka, M. (2003). Pore size distribution of clayey soils measured by mercury intrusion porosimetry and its relation to hydraulic conductivity. *Soils and Foundations*, 43(6), 63–73. [https://doi.org/10.3208/sandf.43.6\\_63](https://doi.org/10.3208/sandf.43.6_63)
- Tarantino, A. (2009). A water retention model for deformable soils. *Géotechnique*, 59(9), 751–762. <https://doi.org/10.1680/geot.7.00118>
- van Genuchten, M. T. (1980). A closed-form equation for predicting the hydraulic conductivity of unsaturated soils. *Soil Science Society of America Journal*, 44(5), 892–898. <https://doi.org/10.2136/sssaj1980.03615995004400050002x>
- Wang, H., Chen, R., Leung, A. K., Garg, A., & Jiang, Z. (2025). Pore-based modeling of hydraulic conductivity function of unsaturated rooted soils. *International Journal for Numerical and Analytical Methods in Geomechanics*, 49(7), 1790–1803. <https://doi.org/10.1002/nag.3958>
- Wang, J. D., Li, P., Ma, Y., Vanapalli, S. K., & Wang, X. G. (2020). Change in pore-size distribution of collapsible loess due to loading and inundating. *Acta Geotechnica*, 15(5), 1081–1094. <https://doi.org/10.1007/s11440-019-00815-9>
- Weynants, M., Vereecken, H., & Javaux, M. (2009). Revisiting Vereecken pedotransfer functions: Introducing a closed-form hydraulic model. *Vadose Zone Journal*, 8(1), 86–95. <https://doi.org/10.2136/vzj2008.0062>
- Wyllie, M., & Gregory, A. (1955). Fluid flow through unconsolidated porous aggregates. *Industrial & Engineering Chemistry*, 47(7), 1379–1388. <https://doi.org/10.1021/ie50547a037>
- Zhang, Y. G., Weihermüller, L., Toth, B., Noman, M., & Vereecken, H. (2022). Analyzing dual porosity in soil hydraulic properties using soil databases for pedotransfer function development. *Vadose Zone Journal*, 21(5), e20227. <https://doi.org/10.1002/vzj2.20227>
- Zhou, C., & Chen, R. (2021). Modelling the water retention behaviour of anisotropic soils. *Journal of Hydrology*, 599, 126361. <https://doi.org/10.1016/j.jhydrol.2021.126361>
- Zhou, C., & Ng, C. W. W. (2014). A new and simple stress-dependent water retention model for unsaturated soil. *Computers and Geotechnics*, 62, 216–222. <https://doi.org/10.1016/j.compgeo.2014.07.012>